Electronic Supplementary Material (ESI) for Journal of Materials Chemistry C.

Supporting Information

for

Heterostructures of skutterudites and germanium antimony tellurides – structure analysis and thermoelectric properties of bulk samples

by

Felix Fahrnbauer, Stefan Maier, Martin Grundei, Nadja Giesbrecht, Markus Nentwig, Tobias Rosenthal, Gerald Wagner, G. Jeffrey Snyder and Oliver Oeckler*

Table of contents

I General information
II Powder X-ray diffraction
III Electron microscopy
IV Structure refinement from single-crystal data
V Thermoelectric measurements
VI References

I General information

The starting materials were used as purchased without further purification for the syntheses listed in Table S1. In order to avoid moisture, Te was kept in an exsiccator over P_4O_{10}.

Profile fits and structure refinements by the Rietveld method were done using TOPAS Academic,[1] based on powder X-ray diffraction patterns (PXRD) and starting structure models from the PCD [2] or ICSD [3] database, respectively.

High-resolution transmission electron microscopy (HRTEM) and selected-area electron diffraction (SAED) data were evaluated using the Digital Micrograph,[4] analySIS [5] and JEMS [6] software; for STEM and EDX data, the programs ES Vision [7] and Genesis [8] were used.

SMART [9] and SAINT [10] were used for indexing and integrating datasets acquired with microfocused synchrotron radiation. Semiempirical absorption correction was done with SADABS.[11] Structure solution and refinement were performed with SHELX-2014,[12] the dispersion correction terms $\Delta f'$ and $\Delta f''$ at $\lambda = 0.29460$ Å were taken from the NIST [13] database.

Table S1 Overview over synthesis conditions and compositions of the samples used in the present study (the single parameters for each full thermoelectric characterization were measured on two or three samples, respectively; many experiments not listed here have shown that different melting times do not influence the results).

nominal composition [§]	used for …	melting at 950 °C	annealing
$[CoSb_3]_{0.5}(GeTe)_2Sb_2Te_3$	PXRD, Fig. S1	2 h	64.5 h @ 530 °C
$[CoSb_2(GeTe)_{0.5}]_{0.6}(GeTe)_5Sb_2Te_3$	PXRD, Fig. 1	2 h	4 h @ 590 °C
$[CoSb_2(GeTe)_{0.5}]_1(GeTe)_{10.5}Sb_2Te_3$	PXRD, Fig. 1 TEM and synchrotron measurements, T-dependent PXRD, Fig. 3 - 4, S2, S4, Tables 1, S2, S4 – S7	2 h	4 h @ 590 °C
$[CoSb_2(GeTe)_{0.5}]_1(GeTe)_{10.5}Sb_2Te_3$	EDX element mapping (SEM), Fig. S3	2 h	--
$[CoSb_2(GeTe)_{0.5}]_{1.3}(GeTe)_{15}Sb_2Te_3$	PXRD, Fig. 1	2 h	4 h @ 590 °C
$[CoSb_3]_{0.5}(GeTe)_{15}Sb_2Te_3$	PXRD, Fig. S1	2 h	64.5 h @ 530 °C
$[CoSb_3]_{0.5}(GeTe)_{17}Sb_2Te_3$	TEM, Fig. S5-6, Table S3	2 h	64.5 h @ 530 °C
$(GeTe)_{10.5}Sb_2Te_3$	T- dependent PXRD, Fig. 2	48 h	0.5 h @ 590 °C
$(GeTe)_{10.5}Sb_2Te_3$	thermoelectric characterization: LFA1000 LSR-3 (NiCr-Ni thermocouples)	4 h 2 h	0.5 h @ 590 °C
$[CoSb_2(GeTe)_{0.5}]_{0.2}(GeTe)_{10.5}Sb_2Te_3$	thermoelectric characterization: LFA1000 and LSR-3 (NiCr-Ni thermocouples)	2 h	0.5 h @ 590 °C
$[CoSb_2(GeTe)_{0.5}]_{0.5}(GeTe)_{10.5}Sb_2Te_3$	thermoelectric characterization: LFA 457 in-house built facility for σ measurements S measurements with W-Nb thermocouples	2 h	0.5 h @ 590 °C
$[CoSb_2(GeTe)_{0.5}]_1(GeTe)_{10.5}Sb_2Te_3$	thermoelectric characterization: LFA 457 in-house built facility for σ measurements S measurements with W-Nb thermocouples	27 h 2.5 h 70 h	0.5 h @ 590 °C
$[CoSb_2(GeTe)_{0.5}]_2(GeTe)_{10.5}Sb_2Te_3$	thermoelectric characterization: LFA 457 in-house built facility for σ measurements S measurements with W-Nb thermocouples	26 h 2.5 h 46 h	0.5 h @ 590 °C

§ Corresponds to the starting composition; possible (additional) side-phases that are not evident from these formulae are discussed in the corresponding sections.

II Powder X-ray diffraction

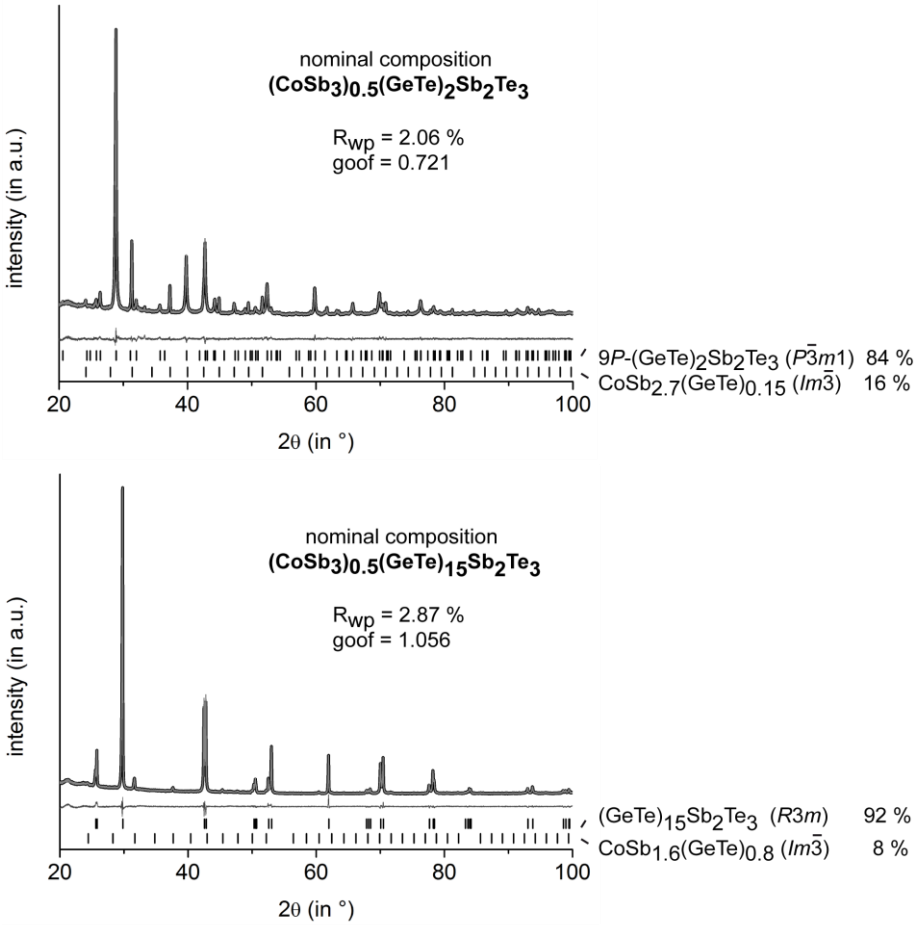

Fig. S1 PXRD patterns of different germanium antimony tellurides (GST materials) with skutterudite-type precipitates (compositions given in the image, all samples annealed at 530 °C for 64.5 h): experimental (black), calculated (light gray) and difference (dark gray) profiles; reflection positions are indicated as vertical lines; residuals and calculated phase fractions are given; structure models taken from [14] ($P\bar{3}m1$), [15] ($R3m$) and [16] ($Im\bar{3}$) [note that the overall fraction of the skutterudite-type phase is not exactly that used for the samples shown in Fig. 1 in the manuscript and that GeTe substitution in $CoSb_3$ was not taken into account; however, Ge exsolution cannot be detected due to the very small amount].

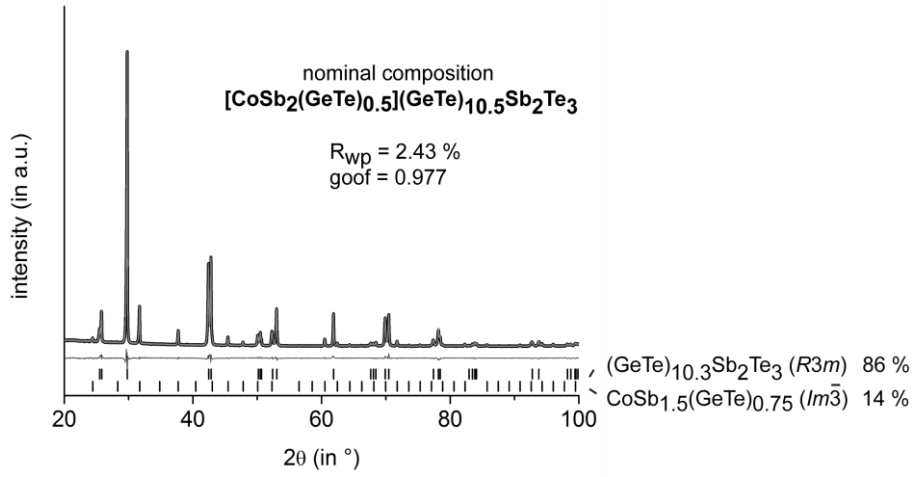

Fig. S2 PXRD pattern of a sample with the nominal composition $[CoSb_2(GeTe)_{0.5}](GeTe)_{10.5}Sb_2Te_3$ as used for single-crystal structure refinements (sample annealed at 590 °C for 4 h): experimental (black), calculated (light gray) and difference (dark gray) profiles; reflection positions are indicated as vertical lines; residuals and calculated phase fractions are given; structure models taken from [15] ($R3m$), and [16] ($Im\bar{3}$).

III Electron microscopy

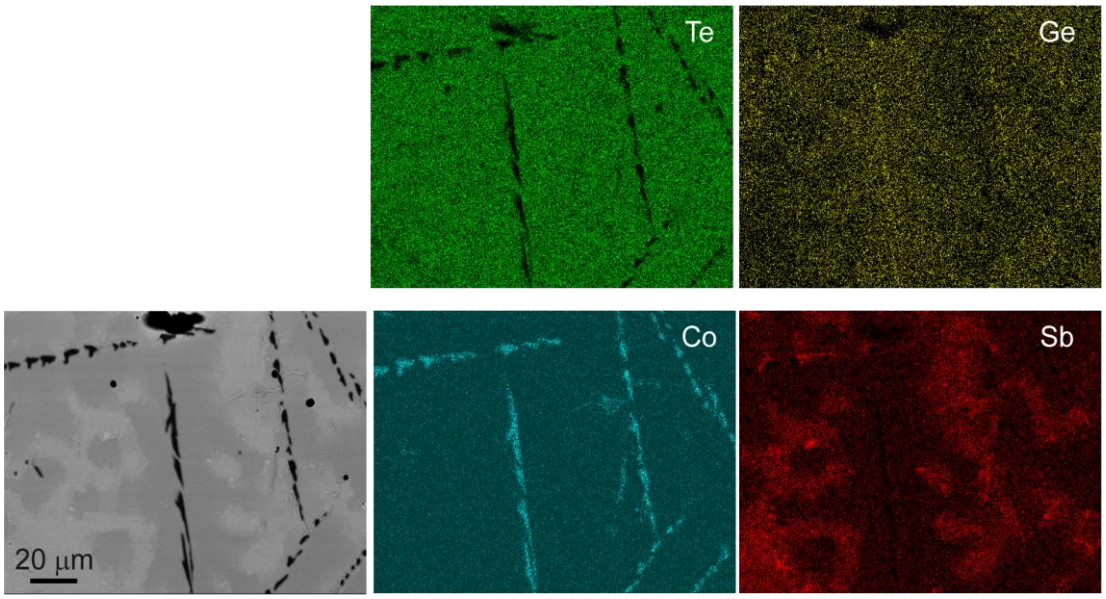

Fig. S3 SEM (scanning electron microscopy) with EDX (energy-dispersive X-ray spectroscopy) element mapping of a sample with the nominal composition $[CoSb_2(GeTe)_{0.5}](GeTe)_{10.5}Sb_2Te_3$ quenched from melt; spatially resolved element distribution for Te and Ge (top row), Co and Sb (bottom row), backscattered electron (BSE) image of the analyzed region (bottom left); no skutterudite-type precipitates were found in quenched samples, but cobalt germanides and small fractions of elemental Co.

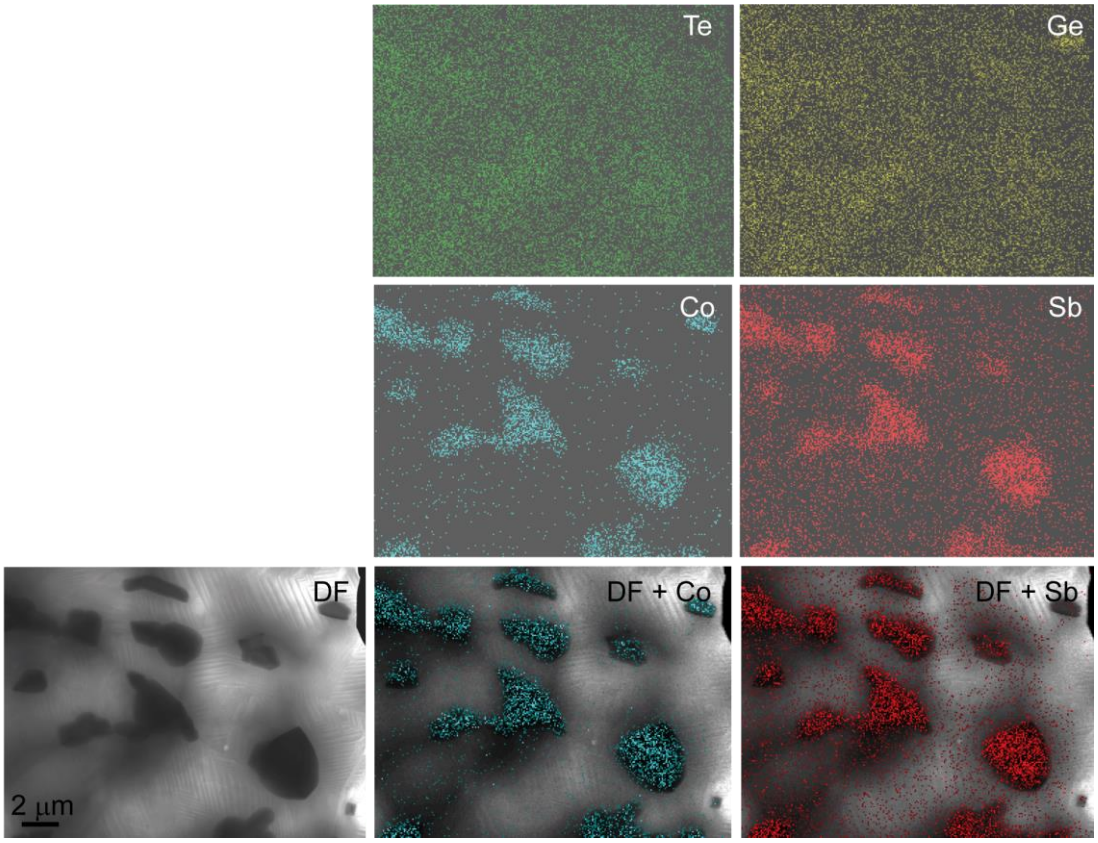

Fig. S4 STEM (scanning transmission electron microscopic) EDX element mapping of a sample with the nominal composition $[CoSb_2(GeTe)_{0.5}](GeTe)_{10.5}Sb_2Te_3$ (annealed at 590 °C for 4 h) as used for single-crystal structure refinements; spatially resolved element distribution for Te and Ge (top row), Co and Sb (middle row), dark-field (DF) image of analyzed region (bottom left) and overlay of DF image with the Co EDX map (bottom, middle) and Sb EDX map (bottom right).

Table S2 SEM-EDX results of a sample with the nominal composition $[CoSb_2(GeTe)_{0.5}](GeTe)_{10.5}Sb_2Te_3$ (used for single-crystal structure refinements); data averaged from 11 and 7 measurement points for $(GeTe)_{10.3}Sb_2Te_3$ and $CoSb_{1.53}(GeTe)_{0.74}$, respectively.

formula	**$(GeTe)_{10.3}Sb_2Te_3$ §**	**$CoSb_{1.53}(GeTe)_{0.74}$ §§**
at.-% meas.	**Ge**: 39.9(6); **Sb**: 9.2(4); **Te**: 51.0(5)	**Co**: 22(2); **Sb**: 43(3); **Ge**: 17(2); **Te**: 18(2)
at.-% calc.	**Ge**: 40.2; **Sb**: 7.8 ; **Te**: 52.0	**Co**: 25.0; **Sb**: 38.0; **Ge**: 18.5; **Te**: 18.5

§ A slightly higher degree of Sb substitution by GeTe in the precipitates as found by TEM (transmission electron microscopic) EDX was taken into account by a slightly lower GeTe content in the calculated formula of the matrix material compared to the nominal formula of the starting material. The assumption of charge neutrality leads to deviations of the calculated formula from the measured one. Excess Sb might lead to a precipitation of Ge (cf. discussion the manuscript). However, no significant fractions of Ge and only traces of cobalt germanides were found.
§§ SEM point measurements exhibit large variation due to X-ray excitation of the material surrounding the microscale precipitates.

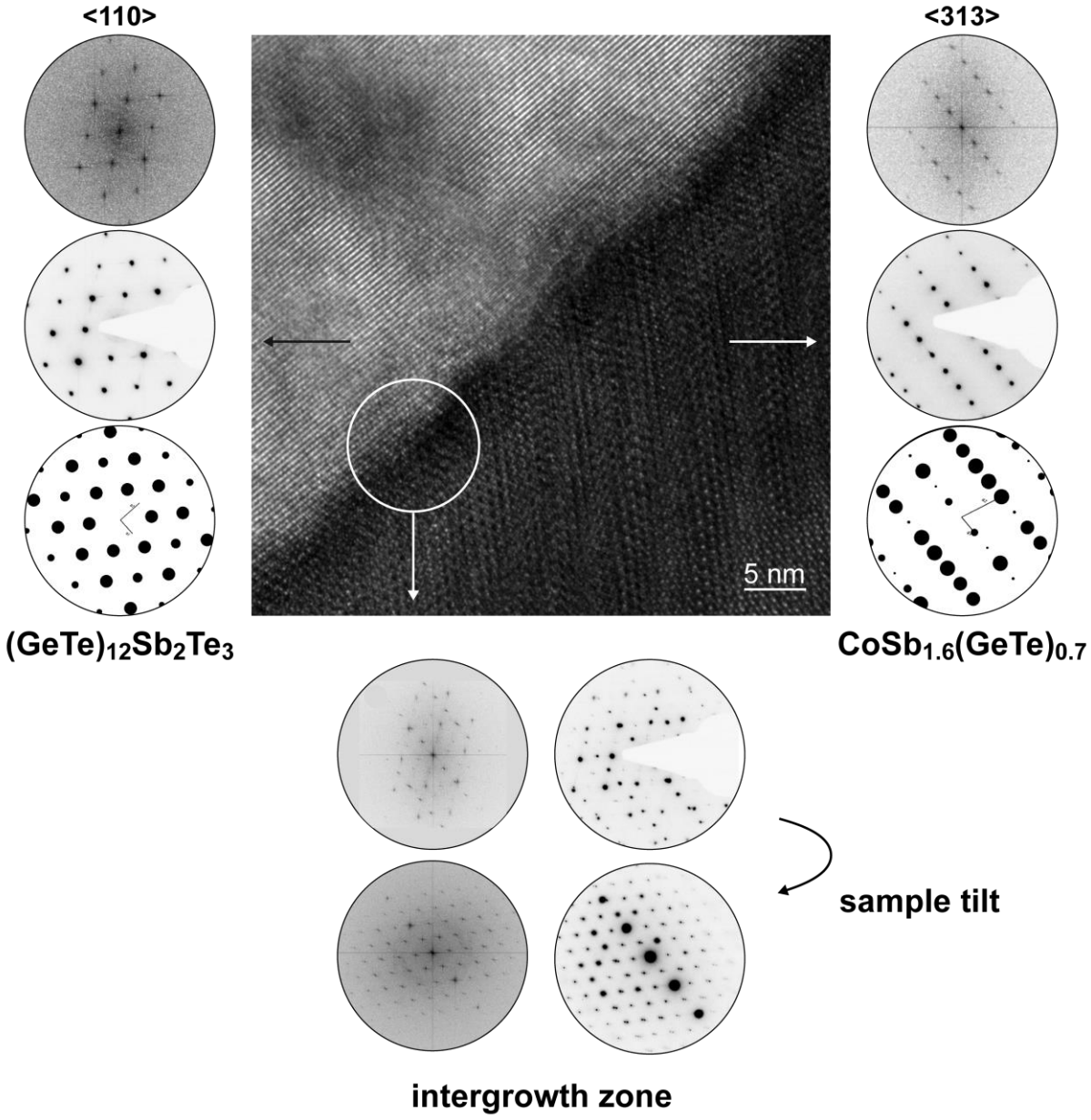

Fig. S5 HRTEM image of overlapping intergrown crystallites (middle) of a sample with the nominal composition $(CoSb_3)_{0.5}(GeTe)_{17}Sb_2Te_3$ (sample annealed for 64.5 h at 530 °C) and corresponding Fourier transforms as well as experimental and simulated SAED patterns (left: rocksalt-type $(GeTe)_{12}Sb_2Te_3$, right: skutterudite-type $CoSb_{1.6}(Ge_0Te)_{0.7}$); bottom: SAED patterns and Fourier transforms of the intergrowth zone in two different orientations; note that the nominal composition of the sample differs from the one used for single-crystal structure refinement.

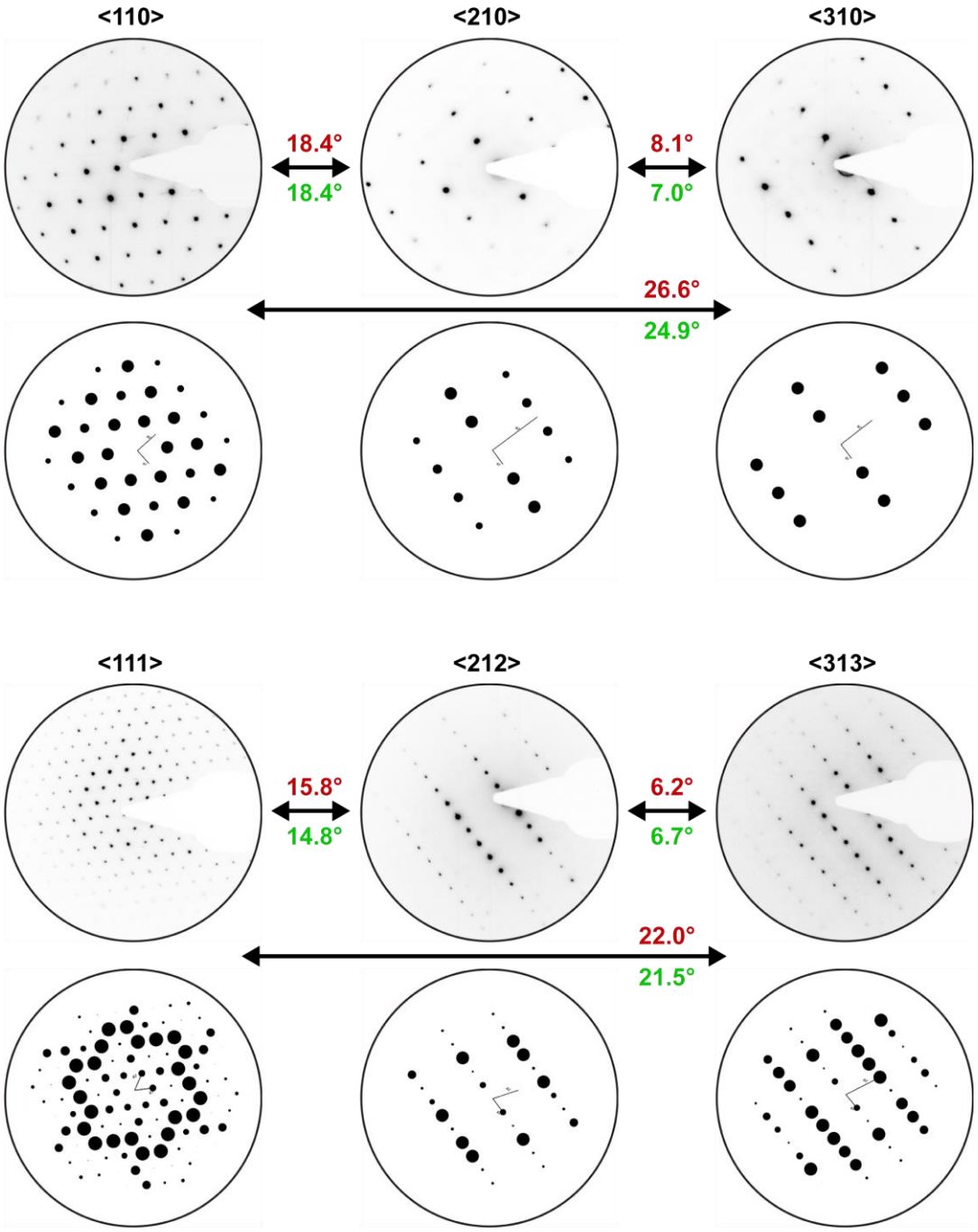

Fig. S6 SAED tilt series with simulated patterns and experimental (red) as well as calculated (green) tilt angles of crystallites from a sample with the nominal composition $(CoSb_3)_{0.5}(GeTe)_{17}Sb_2Te_3$ (sample annealed for 64.5 h at 530 °C, same sample region as in Fig. S5); top: rocksalt-type $(GeTe)_{12}Sb_2Te_3$, bottom: $CoSb_{1.6}(GeTe)_{0.7}$.

Table S3 TEM-EDX results of the components of a sample with the nominal composition $(CoSb_3)_{0.5}(GeTe)_{17}Sb_2Te_3$; data averaged from 3 and 4 measurement points for $(GeTe)_{12}Sb_2Te_3$ and $CoSb_{1.6}(GeTe)_{0.7}$, respectively.

formula	**$(GeTe)_{12}Sb_2Te_3$** [§]	**$CoSb_{1.6}(GeTe)_{0.7}$**
at.-% meas.	**Ge**: 44(2); **Sb**: 7(1); **Te**: 48(2)	**Co**: 24.0(4); **Sb**: 40(2); **Ge**: 19(1); **Te**: 17(1)
at.-% calc.	**Ge**: 41.4; **Sb**: 6.9 ; **Te**: 51.7	**Co**: 25.0; **Sb**: 40.0; **Ge**: 17.5; **Te**: 17.5

[§] Sb substitution in the precipitates was not taken into account in the starting composition but leads to a lower GeTe content in the matrix. $(GeTe)_{12}Sb_2Te_3$ is the approximate composition of the matrix with respect to the incorporation of the substituted Sb of the precipitates as well as the (formally) decreased GeTe content. Small fractions of elemental Ge or cobalt germanides (as a consequence of excess Sb) as found in the PXRD were not examined by means of TEM.

IV Structure refinement from single-crystal data

Table S4 Wyckoff positions, atomic coordinates, site occupancies and equivalent isotropic displacement parameters (U_{eq} = 1/3[U_{11} + U_{22} + U_{33}], in Å^2) for skutterudite-type $CoSb_{1.53}(GeTe)_{0.74}$.

atom	Wyck.	x	y	z	site occupancy factors	U_{eq}
Co1	8*c*	1/4	1/4	1/4	Co 1	0.0083(2)
Sb2/Ge2/Te2	24*g*	1/2	0.34349(4)	0.16459(4)	Sb 0.51(3) Ge 0.247(17) Te 0.247(17)	0.01223(12)

Table S5 Anisotropic displacement parameters (U_{ij}, in Å^2) for skutterudite-type $CoSb_{1.53}(GeTe)_{0.74}$.

atom	U_{11}	U_{22}	U_{33}	U_{12}	U_{13}	U_{23}
Co1	0.0083(2)	= U_{11}	= U_{11}	0.00071(16)	= U_{12}	= U_{12}
Sb2/Ge2/Te2	0.00715(14)	0.01361(16)	0.01591(16)	0	0	-0.00065(10)

Table S6 Wyckoff positions, atomic coordinates, site occupancies and equivalent isotropic displacement parameters (U_{eq} = 1/3[U_{11} + U_{22} + U_{33}], in Å^2) for $Ge_{0.77}Sb_{0.15}Te_1$ = $(GeTe)_{10.3}Sb_2Te_3$.

atom	Wyck.	x	y	z	site occupancy factors	U_{eq}
Ge1/Sb1	3*a*	0	0	0.0203(12)	Ge 0.7693 Sb 0.1538	0.018(4)
Te2	3*a*	0	0	1/2	Te 1	0.0200(15)

Table S7 Anisotropic displacement parameters (U_{ij}, in Å^2) for $Ge_{0.77}Sb_{0.15}Te_1$= $(GeTe)_{10.3}Sb_2Te_3$.

atom	U_{11}	U_{22}	U_{33}	U_{12}	U_{13}	U_{23}
Ge1/Sb1	0.019(6)	= U_{11}	0.016(7)	0.010(3)	0	0
Te2	0.021(4)	= U_{11}	0.018(7)	0.010(2)	0	0

V Thermoelectric measurements

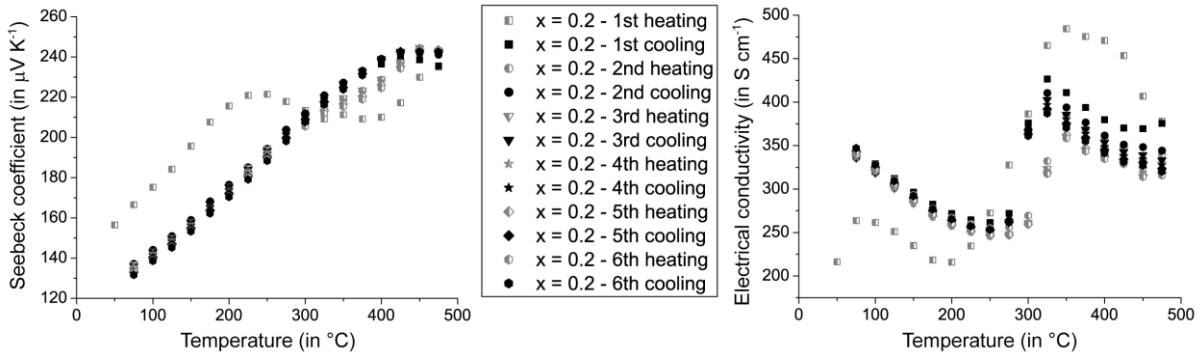

Fig. S7 Seebeck coefficients (left) and electrical conductivities (right) of $[CoSb_2(GeTe)_{0.5}]_{0.2}(GeTe)_{10.5}Sb_2Te_3$ for 6 consecutive heating/cooling cycles.

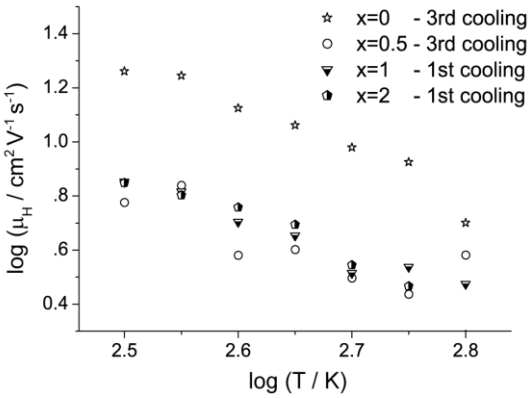

Fig. S8 Decrease of Hall mobility μ_H as a function of temperature (unsmoothed raw data) of $[CoSb_2(GeTe)_{0.5}]_x(GeTe)_{10.5}Sb_2Te_3$ shown by represenative cooling curves, no structural changes occur after first heating (cf. discussion in the manuscript).

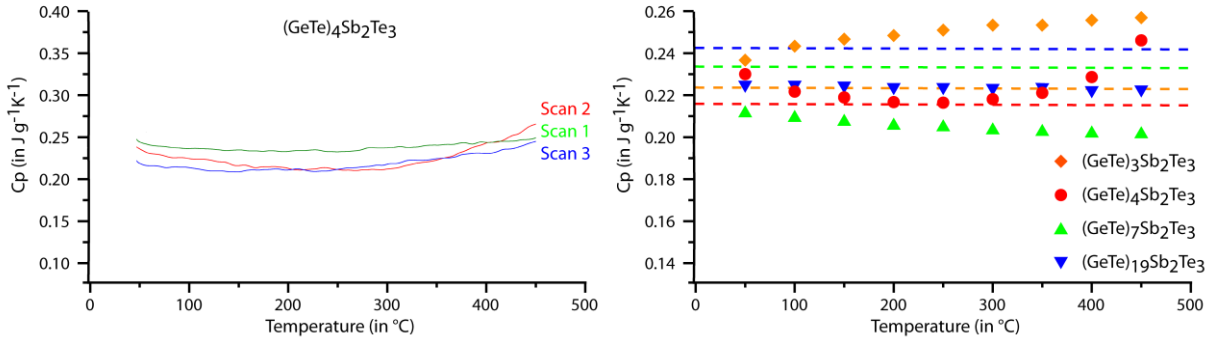

Fig. S9 C_p measurements (DSC) of GST materials (example): three consecutive scans of $(GeTe)_4Sb_2Te_3$ (left) and merged values for $(GeTe)_3Sb_2Te_3$, $(GeTe)_4Sb_2Te_3$, $(GeTe)_7Sb_2Te_3$ and $(GeTe)_{19}Sb_2Te_3$ (right); Dulong-Petit values are given as dashed lines in the corresponding colors; these (so far unpublished) results were obtained in the course of other studies.[17,18]

Cp values were determined for different GST materials using differential scanning calorimetry in the course of previous works,[17,18] where deviations from the Dulong-Petit values (see dashed lines in Fig. S9, right) of up to 15 % - but usually much less - were found at high temperatures. Given the fluctuation of different consecutive C_p measurements on the same sample (Fig. S9, left), these errors appear to be mainly due to the imprecision of the measurements. Thus, the theoretical value calculated according to the Dulong-Petit law can be considered an appropriate approximation that, in these cases, introduces not more error than simple standard C_p measurements.

VI References

1 A. Coelho, TOPAS Academic, version 4.1, Coelho Software, Brisbane, Australia, 2007.

2 P. Villars and K. Cenzual, *Pearson's Crystal Data - Crystal Structure Database for Inorganic Compounds*, ASM International, Materials Park, Ohio, USA, 2009/10.

3 ICSD database*,* version 2006-2, 2007: a) G. Bergerhoff and I. D. Brown, *Crystallographic Databases*, Chester, IUCr, 1987; b) A. Belsky, M. Hellenbrandt, V. L. Karen and P. Luksch, *Acta Crystallogr. Sect. B*, 2002, **58**, 364.

4 DigitalMicrograph, version 3.6.1, Gatan Software, Pleasanton, USA, 1999.

5 analySIS, version 2.1, Olympus Soft Imaging Solutions, Münster, Germany, 1996.

6 a) P. A. Stadelmann, JEMS, version 3.8326 U2012, CIME-EPFL, Lausanne, Switzerland, 2012; b) P. A. Stadelmann, *Ultramicroscopy*, 1987, **21**, 131.

7 ESVision, version 4.0.164, Emispec Systems Inc., Tempe, USA, 1994-2002.

8 Genesis, version 6.1, EDAX, Mahwah, USA, 2010.

9 J. L. Chambers, K. L. Smith, M. R. Pressprich and Z. Jin, SMART, version 5.059, Bruker AXS, Madison, USA, 1997–98.

10 SAINT, version 6.36A, Bruker AXS, Madison, USA, 1997–2002.

11 SADABS, version 2.05, Bruker AXS, Madison, USA, 1999.

12 G. M. Sheldrick, *Acta Crystallogr. Sect. C*, 2015, **71**, 3.

13 C. T. Chantler, K. Olsen, R. A. Dragoset, J. Chang, A. R. Kishore, S. A. Kotochigova and D. S. Zucker, *J. Phys. Chem. Ref. Data*, 1995, **24**, 71.

14 P. Urban, M. N. Schneider, L. Erra, S. Welzmiller, F. Fahrnbauer and O. Oeckler, *CrystEngComm*, 2013, **15**, 4823.

15 L. E. Shelimova, O. G. Karpinskii, M. A. Kretova, V. I. Kosyakov, V. A. Shestakov, V. S. Zemskov and F. A. Kuznetsov, *Inorg. Mater.*, 2000, **36**, 768.

16 D. G. Mandrus, A. Migliori, T. W. Darling, M. F. Hundley, E. J. Peterson and J. D. Thompson, *Phys. Rev. B: Condens. Matter*, 1995, **52**, 4926.

17 T. Rosenthal, M. N. Schneider, C. Stiewe, M. Döblinger and O. Oeckler, *Chem. Mater.,* 2011, **23**, 4349.

18 T. Rosenthal, P. Urban, K. Nimmrich, L. Schenk, J. de Boor, C. Stiewe, and O. Oeckler, *Chem. Mater.,* 2014, **26**, 2567.